

On the Sub-Critical Bifurcation of Anti-Phase and In-Phase Synchronized Vortex Shedding Forms

Yih Ferng Peng

Department of Civil Engineering, National Chi Nan University, Puli 545, Taiwan, China.
Email: yfpeng@ncnu.edu.tw

Received 2013

ABSTRACT

Transition of flows past a pair of side-by-side circular cylinders are investigated by numerical simulations and the bifurcation analysis of the numerical results. Various flow patterns behind the cylinder-pair have been identified by the gap ratio (G) and Reynolds number (Re). This study focus on transition of in-phase and anti-phase vortex shedding synchronized forms. A nested Cartesian-grid formulation, in combination with an effective immersed boundary method and a two-step fractional-step procedure, has been adopted to simulate the flows. Numerical results reveal that the in-phase and anti-phase vortex shedding flows at $Re = 100$ can co-exist at $2.08 \leq G \leq 2.58$. Hysteresis loop with increasing/decreasing G at constant Reynolds number $Re = 100$ is reported.

Keywords: In-phase Vortex Shedding; Anti-phase Vortex Shedding; Hysteresis

1. Introduction

Because of its fundamental importance and engineering significance, unstable flow interferences across bluff bodies have been investigated extensively. Flow interference with a pair of cylinders is complex in which both relative-gap between the cylinders and arrangements of relative position (in tandem, side-by-side, or in staggered) play crucial roles in the physical transition. Among flows around a pair of cylinders in various configurations, those behind circular cylinders in a side-by-side arrangement have been mostly extensively studied [1-11]. It is now well established that the flow patterns behind a pair of side-by-side cylinders can be classified [3,12] by the gap-ratio G (surface-to-surface distance divided by cylinder-diameter) and the Reynolds number (Reynolds number, Re , is defined as $Re = U_o D / \nu$, where U_o is the free-stream velocity, D is the cylinder diameter, and ν is the kinematic viscosity). At very small Gap ratios, the two cylinders may behave in a similar fashion to a single bluff-body [1]. At intermediate Gap ratios, the two side-by-side cylinders is known [2] to exhibit a deflected or biased flow patterns, which are bi-stable in nature. The deflected flow pattern is characterized by a gap flow biased towards one of the two cylinders. The gap flow in this regime switches spontaneously from one side to the other and thus corresponds to the flip-flopped regime [5]. For weak coupling (with relatively large G , $1 \leq G \leq 5$) many of the past researchers report occurrences of both anti-phase and in-phase synchronized vortex shedding

behind a pair of circular cylinders. Findings of Williamson [4] confirm that the shedding vortices (for $40 \leq Re \leq 160$) remain synchronized either in phase or in anti-phase. Anti-phase streets often preserve the phase-locked identity of the vortices even at a far downstream location. However, for strong coupling (with relatively lower G) only in-phase vortex shedding has been reported, and the associated physical process eventually leads to formation of a complex asymmetrically evolving Benard von Karman streets.

Although there are varieties of flow patterns behind a pair of side-by-side cylinders have been identified (which include semi-single and twin vortex street formations, symmetric and deflected flows, stationary, biased and flip-flopped-type vortex shedding, periodic, quasi-periodic, and weakly-chaotic flows, and in-phase and anti-phase vortex synchronizations), very restriction results have been reported on transition of those various flow patterns. Examples can be found in the studies of Mizushima & Ino [13] and Peng *et al.* [14]. In [13], parameter space of the gap ratio and the critical Reynolds number of symmetry/deflected vortex shedding flows and in-phase/anti-phase vortex shedding flows behind a pair of circular cylinders at low Reynolds number have been reported by results of numerical simulations and linear stability analyses. While in the study [14], transition from semi-single symmetry vortex shedding flow to semi-single deflected vortex shedding flow as well as transition from twin symmetry vortex shedding to twin deflected vortex shedding and then transition to the flipped-

flopped vortex shedding regime behind a pair of elliptical cylinders at low Reynolds number are shown by results of direct numerical simulations. Although there are a lot of experimental and numerical studies on the side-by-side cylinders, the important transition phenomenon from in-phase to anti-phase vortex shedding synchronization and *vs.* are still unclear. Purpose of this study is then focus on transition of in-phase/anti-phase vortex shedding synchronized forms behind a pair of side-by-side circular cylinders. High resolution numerical methods based on a nested Cartesian grid formulation, in combination with an effective immersed boundary method and a two-step fractional-step procedure, have been adopted to simulate flows past a pair of side-by-side circular cylinders. Hysteresis loop with increasing/decreasing *Re* at constant gap ratio describing the hysteresis phenomenon of in-phase/anti-phase vortex shedding synchronized forms are reported.

2. Numerical Methods and Validations

In this study, transitions of in-phase and anti-phase vortex shedding flows behind a pair of circular cylinders in the side-by-side arrangement are numerically investigated. A nested Cartesian-grid formulation, in combination with an effective immersed boundary method and a two-step fractional-step procedure, has been adopted to simulate the flows. Extensive related details of the discretization schemes consisting of inside fine/coarse grid-areas and the associated immersed boundary method may be found in Peng *et al.* [14-15].

Here we briefly describe the implemented numerical method. Governing equations used are unsteady incompressible Navier–Stokes equations in primitive variables. In integral forms, the dimensionless governing equations (with lengths normalized by the diameter *D* of cylinders, velocities normalized by the uniform inflow velocity *U*₀, and time by *D/U*₀) appear as the following.

The mass conservation equation

$$\int_{CS} \bar{u} \cdot \bar{n} \, dS = 0, \tag{1}$$

and the momentum conservation equation

$$\begin{aligned} & \frac{\partial}{\partial t} \int_{CV} \bar{u} dV + \int_{CS} \bar{u} (\bar{u} \cdot \bar{n}) dS \\ & = - \int_{CS} p \bar{n} dS + \frac{1}{Re} \int_{CS} \nabla \bar{u} \cdot \bar{n} dS \end{aligned} \tag{2}$$

CS and *CV* in Eqs. (1) and (2) denote the control-surface and control-volume, respectively, and \bar{n} is a unit vector normal to the control-surface. While advancing in time, a second order accurate two-step fractional-step method is used. A second-order Adams-Bashforth scheme is employed for discretizing the convective terms, and diffusion terms are discretized using an implicit Crank

Nicolson scheme.

In the iterations of the discretized equations, a local grid refinement technique is adopted through the introduction of two nested blocks in the computational domain. The implemented nested-block finite-volume based Cartesian-grid method is noted to facilitate effective/accurate simulation of the presently investigated unsteady viscous incompressible flows past multiple immersed boundaries. The procedure adopted here allows systematic simulation of flows past the cylinder-pair, and preserves global second-order accuracy [15]. A sketch for the computational domain with implemented boundary conditions and a side-by-side arrangement of cylinder-pair is provided in **Figure 1**. Various domain-lengths used for simulations under the present study are defined as: *L*₁ = 5*D*, *L*₂ = 50*D*, *L*₃ = 12*D*, *L*₄ = 4*D*, *L*₅ = 8*D*, and *L*₆ = 5.5*D*, facilitating generation of a physical domain of size 55*D* × 24*D*, consisting an inner fine-grid (*Grid 2*) area 12*D* × 11*D*. Upon taking $\Delta x = \Delta y = 0.1D$ for the outer *Grid 1* (the coarse grid), and $\Delta x = \Delta y = 0.05D$ for the inner *Grid 2*, the total grid size became 168,000, with *Grid 1* = 120,000, and *Grid 2* = 48,000.

The simple concept of immersed boundary (*IB*) method adopted here helps to simulate effectively the wake evolutions past the cylinders. The virtual presence of the cylinders within the flow domain is facilitated by introducing a locally active distributed body force in the Navier-Stokes equation, *i.e.*,

$$\frac{\partial \bar{u}}{\partial t} = -(\bar{u} \cdot \nabla) \bar{u} - \nabla p + \frac{1}{Re} \Delta \bar{u} + \bar{f},$$

in which the distributed body force \bar{f} is defined as $\bar{f} \equiv ((\bar{u} \cdot \nabla) \bar{u} + \nabla p - 1/Re \times \Delta \bar{u}) \times \phi$, and ϕ represents the volume-fraction of the solid body within a computational cell. For a cell entirely occupied by the cylinders, $\phi = 1$ is used; and for a cell fully occupied by fluid, $\phi = 0$ is taken. However, for an interface-cell, partially occupied by a cylinder and partially by fluid, $0 < \phi < 1$ is devoted. Thereafter, the governing equations are solved everywhere in the computational domain, including cells which are occupied by the elliptic cylinders.

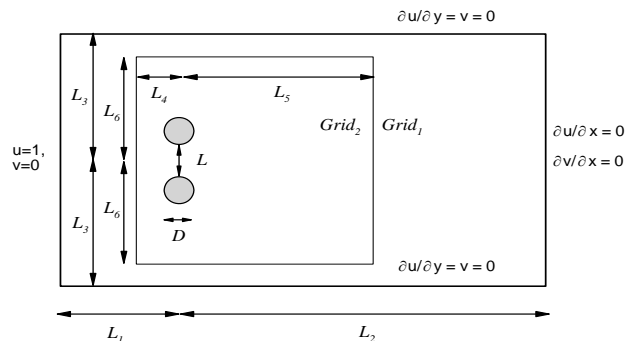


Figure 1. Schematic plot of the flow domain.

It is noted that an extensive validation of the underlying method has been well-documented in [14-15]. In [14], computations of important critical Reynolds numbers ($Re_{cr,v}$) that correspond to onsets of vortex shedding for uniform flows past a circular cylinder, an elliptical cylinder, and two side-by-side attached elliptical cylinders were performed. As listed on **Table 1**, for a circular cylinder, our previous study observed this $Re_{cr,v}$ to be 47.2, which compares quite well with the experimentally predicted values 46.9 - 47.9 [16-18], and the theoretical values 46.1 - 47.3, as obtained by those linear stability analysis [19-20] and the bifurcation analysis of Dusek *et al.* [21].

3. Results

3.1. Overview of Flows behind a Pair of Side-by-Side Circular Cylinders

This study begins with the investigation of critical transition characteristics in the narrow gap range, and extracts the underlying bifurcation patterns. For this, first, flow properties past two side-by-side circular cylinders in the gap-ratio range $0.2 \leq G \leq 3.0$ and $40 \leq Re \leq 100$ are extensively simulated. The observed distinctive physical properties of these flows are sequentially characterized in **Table 2**, in which $\bar{V}_{C,x=1.5}$ denotes the time-averaged transverse velocity at $(x, y) = (1.5, 0.0)$, $C_{L,1+2}$ is the temporal combined lift-coefficient (subscript 1 + 2 denotes upper plus lower cylinder effects, *i.e.*, $C_{L,1+2} = C_{L1} + C_{L2}$), and T is the period of vortex shedding. “Flow types” (last column, **Table 2**) are classified based on the following three special characteristics. The first letter in the abbreviated flow-type, “S,” corresponds to the *semi-single flow*, and “T” corresponds to *twin flow*. For the second letter, “S” represents *symmetric flow*, and “D” denotes the *deflected flow*. In the third and fourth places, “SS” indicates *steady-state flow*, “VP” represents *periodic vortex shedding flow*, “VQ” stands for *quasi-periodic vortex shedding flow*, and “VC” denotes the *chaotic vortex shedding*. Various vortex shedding regimes, including flip-flopped, in-phase, and anti-phase vortex shedding flows are also denoted by superscripts in last column. From the simulated data, the readers may note that at all Reynolds.

Table 1. Critical Reynolds number of onset of vortex shedding for flow past a circular cylinder.

Source	$Re_{cr,v}$	Analytic Method
Present	47.2	bifurcation analysis
Provansal <i>et al.</i> [16]	47.0	experiments
Williamson [17]	47.9	experiments
Norberg [18]	47.4 (± 0.5)	experiments
Jackson [19]	46.2	linear stability analysis
Kumar & Mittal [20]	47.3	linear stability analysis
Dusek <i>et al.</i> [21]	46.1	bifurcation analysis

Table 2. Simulated results of flows past two side-by-side circular cylinders at $40 \leq Re \leq 100$ and $0.2 \leq G \leq 3.0$.

No.	G	Re	$\bar{V}_{C,x=1.5}$	$C_{L,1+2}$	T	Flow type
1	0.2	40	0.0	0.593	10.80	S,S,VP
2	0.2	60	0.0	0.921	9.75	S,S,VP
3	0.2	80	0.0	0.786	9.20	S,S,VP
4	0.2	100	0.0	0.258	9.08	S,S,VP
5	0.4	40	0.0	0.005	13.61	S,S,VP
6	0.4	60	0.111	0.001	12.76	S,D,VP
7	0.4	80	0.0	NA	NA	S,S,VQ ^F
8	0.4	100	0.0	NA	NA	S,S,VC ^F
9	0.6	40	0.0	0.0	∞	T,S,SS
10	0.6	60	0.0	0.0	∞	T,S,SS
11	0.6	80	0.0	NA	∞	T,S,VC ^F
12	0.6	100	0.0	NA	∞	T,S,VC ^F
13	0.8	40	0.0	0.0	∞	T,S,SS
14	0.8	60	0.0	NA	NA	T,S,VQ ^F
15	0.8	80	0.0	NA	NA	T,S,VC ^F
16	0.8	100	0.0	NA	NA	T,S,VC ^F
17	1.0	40	0.0	0.0	∞	T,S,SS
18	1.0	60	0.0	NA	NA	T,S,VQ ^F
19	1.0	80	0.0	NA	NA	T,S,VQ ^F
20	1.0	100	0.0	NA	NA	T,S,VC ^F
21	1.2	40	0.0	0.0	∞	T,S,SS
22	1.2	60	0.0	NA	NA	T,S,VQ ^F
23	1.2	80	0.0	NA	NA	T,S,VQ ^F
24	1.2	100	0.0	NA	NA	T,S,VQ ^F
25	1.4	40	0.0	0.0	∞	T,S,SS
26	1.4	60	0.0	NA	NA	T,S,VQ ^F
27	1.4	80	0.0	0.439	5.53	T,S,VP ^I
28	1.4	100	0.0	0.622	5.23	T,S,VP ^I
29	1.6	40	0.0	0.0	∞	T,S,SS
30	1.6	60	0.0	NA	NA	T,S,VQ ^F
31	1.6	80	0.0	0.415	5.50	T,S,VP ^I
32	1.6	100	0.0	0.588	5.19	T,S,VP ^I
33	1.8	40	0.0	0.0	∞	T,S,SS
34	1.8	60	0.0	NA	NA	T,S,VQ ^F
35	1.8	80	0.0	0.402	5.45	T,S,VP ^I
36	1.8	100	0.0	0.570	5.13	T,S,VP ^I
37	2.0	40	0.0	0.0	∞	T,S,SS
38	2.0	60	0.0	0.197	6.05	T,S,VP ^I
39	2.0	80	0.0	0.398	5.47	T,S,VP ^I
40	2.0	100	0.0	0.564	5.15	T,S,VP ^I
41	2.2	40	0.0	0.0	∞	T,S,SS
42	2.2	60	0.0	0.192	6.04	T,S,VP ^I
43	2.2	80	0.0	0.399	5.50	T,S,VP ^I
44	2.2	100	0.0	0.0	5.00	T,S,VP ^A
45	2.4	40	0.0	0.0	∞	T,S,SS
46	2.4	60	0.0	0.196	6.06	T,S,VP ^I
47	2.4	80	0.0	0.406	5.56	T,S,VP ^A
48	2.4	100	0.0	0.0	5.04	T,S,VP ^A
49	2.6	40	0.0	0.0	∞	T,S,SS
50	2.6	60	0.0	0.200	6.11	T,S,VP ^I
51	2.6	80	0.0	0.0	5.37	T,S,VP ^A
52	2.6	100	0.0	0.0	5.10	T,S,VP ^A
53	2.8	40	0.0	0.0	∞	T,S,SS
54	2.8	60	0.0	0.208	6.08	T,S,VP ^I
55	2.8	80	0.0	0.0	5.41	T,S,VP ^A
56	2.8	100	0.0	0.0	5.11	T,S,VP ^A
57	3.0	40	0.0	0.0	∞	T,S,SS
58	3.0	60	0.0	0.0	5.94	T,S,VP ^A
59	3.0	80	0.0	0.0	5.49	T,S,VP ^A
60	3.0	100	0.0	0.0	5.17	T,S,VP ^A

numbers ($Re \geq 40$) the single vortex shedding street is reached in the range $G \leq 0.4$. However, for larger G ($G \geq 0.6$), the approach to the vortex shedding flow remained dependent on Re . The flip-flopped vortex-shedding occurred in the gap-ratio range $0.4 \leq G \leq 1.8$ with $Re \geq 60$. In-phase vortex shedding is detected at $0.4 \leq G \leq 1.8$, and anti-phase vortex shedding is founded at large G ($G \geq 2.2$). Notably, while **Table 2** presents the explicit physical details of various flows, for the sake of facilitating immediate comprehension of a trend, the parameter space diagram is suitably summarized in **Figure 2**. As shown in **Figure 2**, it is clear that flows are semi-single at $G < 0.5$. At intermediate Gap ratios the two side-by-side cylinders is known to exhibit a deflected or biased flow patterns, which are bi-stable in nature. The deflected jets through circular gap are further affected by the shedding vortices at higher Re and flows become flip-flopped consequently. The range of Gap ratios where the flip-flopped flow pattern is observed extends from approximately Gap ratios between 0.4 - 1.8 depending on the Reynolds number. At higher Gap ratios, *i.e.*, the cylinders are spaced sufficiently far apart, the pair of cylinders may behave as two independent bluff bodies. Proximity interference effects, however, lead to various modes of synchronization, anti-phase and in-phase, in the vortex formation and shedding processes and the resulting parallel vortex streets. For example, in-phase and anti-phase vortex shedding flows at $Re = 100$ are clearly revealed at $G = 2.0$ and $G = 3.0$, respectively.

3.2. Hysteresis Scenario of In-phase and Anti-phase Synchronized Forms

To investigated the transition of in-phase and anti-phase synchronized forms in flows past a pair of side-by-side circular cylinders, two sets of computations including anti-phase and in-phase branches are carried out. The anti-phase branch started from the anti-phase vortex

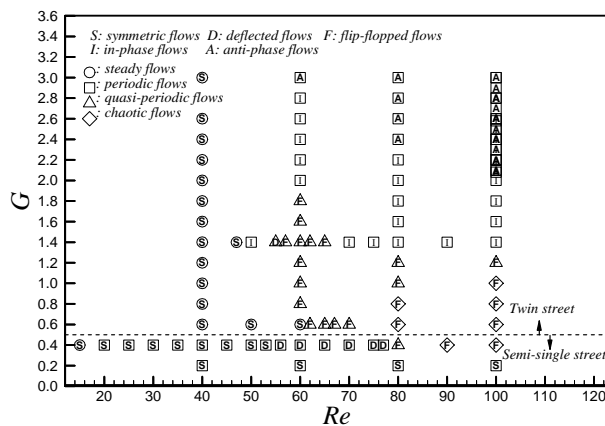


Figure 2. Simulated different wake patterns observed behind two side-by-side circular cylinders.

shedding flow at $G = 3.0$ and $Re = 100$ and are calculated by progressively decreasing G in very small steps. In the meanwhile, the in-phase branch started from the in-phase vortex shedding flow at $G = 2.0$ and $Re = 100$ and are calculated by progressively increasing G in small steps. The observed distinctive physical properties of these flows are sequentially characterized in **Table 3**. It is noted that in anti-phase branch, the solution at a higher G is used as the initial condition for the next lower G . Similarly, in in-phase branch, the solution at a lower G is used as the initial condition for the next higher G .

The flow past cylinder-pair at constant Reynolds number ($Re = 100$) retains anti-phase vortex shedding synchronized forms at high gap ratio ($2.08 \leq G \leq 3.0$), as indicated by our extracted data on **Table 3(a)**. Once G is decreased to $G = 2.06$, the anti-phase vortex shedding flow transits to the in-phase synchronized vortex shedding form. For clarity, the existence of the anti-phase vortex shedding flow pattern at $Re = 100$, and $G = 2.32$ is exhibited in **Figure 3**. It reveals clearly the anti-phase vortex shedding behavior of the simulated flow in the sub-domain $x = [-5, 50]$, $y = [-9, 9]$. The continuation of zero central-line velocity (**Figure 3(d)**), and perfectly anti-phase synchronized growth of the lift ($C_{L,1}$, $C_{L,2}$) coefficients (**Figures 3(b)** and **(c)**) ensure the inherent anti-phase characteristic of vortex shedding (**Figure 3(a)**) in the wake. Note that, unlike for in-phase vortex shedding flow (**Figure 4**), the equal but opposite natured variations of $C_{L,1}$ and $C_{L,2}$ in the present case contribute to the continued vanishing of $C_{L,1+2}$ (**Figure 3(d)**) during the entire time-evolution.

Upon maintaining anti-phase synchronized vortex shedding forms with the past findings related to side-by-side cylinder-pair ($Re = 100$, $2.08 \leq G \leq 3.0$), once the gap-ratio was subsequently increased (from $G = 2.0$), the in-phase synchronized vortex shedding were encountered behind the cylinder-pair ($Re = 100$, $2.0 \leq G \leq 2.58$). The distinguishable physical characteristics associated with the in-phase vortex shedding flows past the cylinder-pair at $Re = 100$ and again $G = 2.32$ is extracted in **Figure 4**. It can be noted from the figure that the gap-flow quickly lost stability; however, the shedding vortices appeared clearly in-phase synchronized at least up to $x \leq 12$. Thereafter, instability is seen to quickly grow, leading to the development of a combined binary vortex street within $12 < x < 26$, and beyond that there occurred an irregular flow pattern over a conversion point. Physical details of this in-phase flow in terms of enhanced $C_{L,1+2}$, and significantly modulated transient evolution (in-phase) of individual lift ($C_{L,1}$ and $C_{L,2}$) coefficients are extracted in **Figures 4(d)**, **(b)** and **(c)**.

3.3. Hysteresis Loop

From the simulated data on **Table 3**, the reader may note that at constant Reynolds number ($Re = 100$), the anti-

phase branch ranges between $2.08 \leq G \leq 3.00$, and the in-phase branch ranges between $2.0 \leq G \leq 2.58$. In the other word, the anti-phase and in-phase synchronized forms behind a pair of circular cylinders ($Re = 100$) can co-exist at $2.08 \leq G \leq 2.58$. The co-existences of the anti-phase and in-phase vortex shedding flow patterns (at $Re = 100$ and $G = 2.32$) have been shown in **Figures 3** and **4**, respectively. **Figures 3(a)** and **4(a)** reveal the anti-phase and in-phase synchronized vortex shedding forms, respectively, by iso-vorticity plots of the flows. The persistence of symmetric flow nature (having zero time mean central-line transverse velocity and lift-coefficient) in both anti-phase and in-phase vortex shedding flows are clearly reflected by the time histories of $C_{L,1+2}$ (**Figures 3(d)** and **4(d)**). However, an enlarged view of individual lift-coefficients ($C_{L,1}$, $C_{L,2}$) for the upper and the lower

Table 3. (a). Numerical results of flow past a pair of side-by-side circular cylinders by decreasing G slowly ($Re = 100$). * denotes the computed case where transition is happen; (b) Numerical results of flow past a pair of side-by-side circular cylinders by increasing G slowly ($Re = 100$). * denotes the computed case where transition is happen.

(a)						
No.	G	Re	$\bar{V}_{C,x=1.5}$	$C_{L,1+2}$	T	Flow type
1	3.00	100	0.0	0.0	5.54	T,S,VP^A
2	2.60	100	0.0	0.0	5.13	T,S,VP^A
3	2.56	100	0.0	0.0	5.13	T,S,VP^A
4	2.54	100	0.0	0.0	5.13	T,S,VP^A
5	2.52	100	0.0	0.0	5.13	T,S,VP^A
6	2.50	100	0.0	0.0	5.12	T,S,VP^A
7	2.48	100	0.0	0.0	5.12	T,S,VP^A
8	2.46	100	0.0	0.0	5.11	T,S,VP^A
9	2.44	100	0.0	0.0	5.11	T,S,VP^A
10	2.42	100	0.0	0.0	5.09	T,S,VP^A
11	2.40	100	0.0	0.0	5.06	T,S,VP^A
12	2.38	100	0.0	0.0	5.09	T,S,VP^A
13	2.36	100	0.0	0.0	5.09	T,S,VP^A
14	2.34	100	0.0	0.0	5.10	T,S,VP^A
15	2.32	100	0.0	0.0	5.08	T,S,VP^A
16	2.30	100	0.0	0.0	5.04	T,S,VP^A
17	2.28	100	0.0	0.0	5.08	T,S,VP^A
18	2.26	100	0.0	0.0	5.06	T,S,VP^A
19	2.24	100	0.0	0.0	5.09	T,S,VP^A
20	2.22	100	0.0	0.0	5.04	T,S,VP^A
21	2.20	100	0.0	0.0	5.03	T,S,VP^A
22	2.18	100	0.0	0.0	5.05	T,S,VP^A
23	2.16	100	0.0	0.0	5.04	T,S,VP^A
24	2.14	100	0.0	0.0	5.08	T,S,VP^A
25	2.12	100	0.0	0.0	5.04	T,S,VP^A
26	2.10	100	0.0	0.0	5.02	T,S,VP^A
27	2.08	100	0.0	0.003	5.00	T,S,VP^A
28*	2.06	100	0.0	0.659	5.21	T,S,VP^I
29	2.04	100	0.0	0.665	5.21	T,S,VP^I

(b)						
No.	G	Re	$\bar{V}_{C,x=1.5}$	$C_{L,1+2}$	T	Flow type
30	2.02	100	0.0	0.665	5.18	T,S,VP^I
31	2.04	100	0.0	0.665	5.21	T,S,VP^I
32	2.06	100	0.0	0.659	5.21	T,S,VP^I
33	2.08	100	0.0	0.651	5.19	T,S,VP^I
34	2.10	100	0.0	0.563	5.15	T,S,VP^I
35	2.12	100	0.0	0.664	5.20	T,S,VP^I
36	2.14	100	0.0	0.664	5.22	T,S,VP^I
37	2.16	100	0.0	0.659	5.21	T,S,VP^I
38	2.18	100	0.0	0.651	5.19	T,S,VP^I
39	2.20	100	0.0	0.564	5.15	T,S,VP^I
40	2.22	100	0.0	0.664	5.20	T,S,VP^I
41	2.24	100	0.0	0.665	5.19	T,S,VP^I
42	2.26	100	0.0	0.660	5.20	T,S,VP^I
43	2.28	100	0.0	0.653	5.20	T,S,VP^I
44	2.30	100	0.0	0.566	5.15	T,S,VP^I
45	2.32	100	0.0	0.665	5.20	T,S,VP^I
46	2.34	100	0.0	0.666	5.20	T,S,VP^I
47	2.36	100	0.0	0.662	5.20	T,S,VP^I
48	2.38	100	0.0	0.655	5.20	T,S,VP^I
49	2.40	100	0.0	0.569	5.16	T,S,VP^I
50	2.42	100	0.0	0.667	5.20	T,S,VP^I
51	2.44	100	0.0	0.669	5.20	T,S,VP^I
52	2.46	100	0.0	0.665	5.20	T,S,VP^I
53	2.48	100	0.0	0.658	5.20	T,S,VP^I
54	2.50	100	0.0	0.572	5.13	T,S,VP^I
55	2.52	100	0.0	0.670	5.20	T,S,VP^I
56	2.54	100	0.0	0.672	5.20	T,S,VP^I
57	2.56	100	0.0	0.668	5.20	T,S,VP^I
58	2.58	100	0.0	0.662	5.20	T,S,VP^I
59*	2.60	100	0.0	0.0	5.13	T,S,VP^A

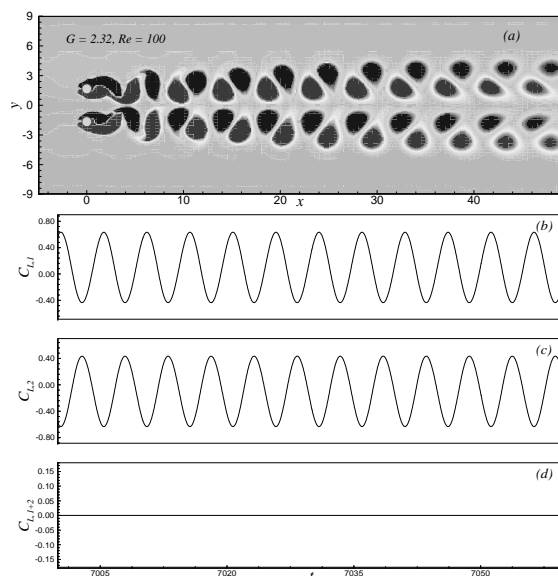


Figure 3. The simulated anti-phase flow at $G = 2.32$ and $Re = 100$. (a) Observed anti-phase flow pattern. Time-histories of: (b) $C_{L,1}(t)$; and (c) $C_{L,2}(t)$. (d) Vanishing of the combined lift-coefficient $C_{L,1+2}$.

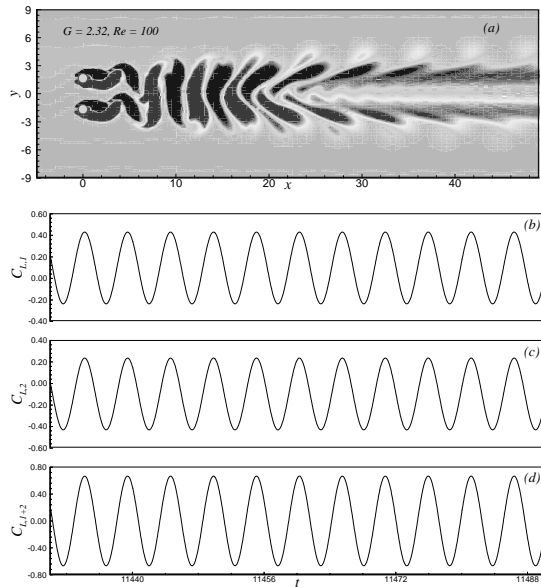


Figure 4. The simulated periodic in-phase flow at $G = 2.32$ and $Re = 100$. (a) In-phase vortex shedding behavior. Time-histories of: (b) $C_{L,1}(t)$; and (c) $C_{L,2}(t)$. (d) Enhancement of the combined lift-coefficient $C_{L,1+2}$.

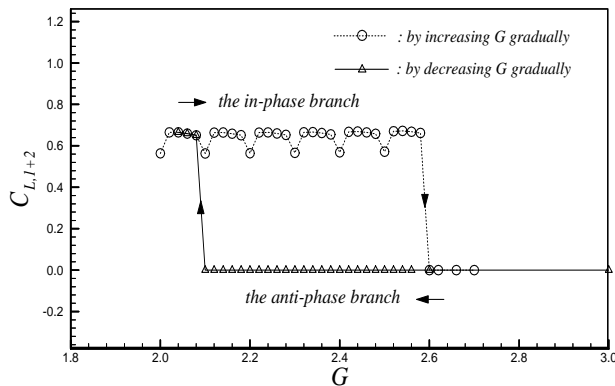


Figure 5. The hysteresis region with G of in-phase and anti-phase synchronized vortex shedding forms for flows past a pair of circular cylinders at $Re = 100$.

cylinders (Figures 3(b) and (c)/Figures 4(b) and (c)) reveals occurrence of anti-phase/in-phase vortex shedding vortices of the upper and lower vortex streets. Readers may note that the corresponding lift-amplitudes ($C_{L,1+2}$) in anti-phase vortex shedding flows become neutralized as shown in Figure 3(d), on the contrary, the corresponding lift-amplitudes ($C_{L,1+2}$) in in-phase vortex shedding flows become enhanced as shown in Figure 4(d), respectively. Since the value of $C_{L,1+2}$ stands as a characteristic value of anti-phase/in-phase synchronized vortex shedding forms, it is worthy to show the $C_{L,1+2}$ distributions. As shown in Figure 5, the $C_{L,1+2}$ distribution along the anti-phase branch ($C_{L,1+2} = 0$) combines the in-phase branch ($C_{L,1+2} \neq 0$) becomes a hysteresis loop. Particularly, the anti-phase branch starting from G

$= 3.0$ trace along a straight segment, ending at $G = 2.08$, and then merges to the in-phase branch. While the in-phase branch starting from $G = 2.0$ trace along a wavy line, ending at $G = 2.58$, and then merges to the anti-phase branch.

4. Conclusions

Numerical results have been presented for the in-phase and anti-phase vortex shedding synchronized forms of flows behind a pair of side-by-side circular cylinders. Flows are restricted in low-Reynolds-number ($Re \leq 100$) laminar regime for various small/middle gap ratio ($0.2 \leq G \leq 3.0$). The computations have been carried out in two-dimensional, using a high resolution numerical method based on a nested Cartesian grid formulation, in combination with an effective immersed boundary method and a two-step fractional-step procedure.

Hysteresis phenomenon of the in-phase/anti-phase vortex shedding synchronized forms of flows has been studied in detail. For flows behind a pair of side-by-side circular cylinders at $Re = 100$, the hysteresis loop with width ranges between $2.08 \leq G \leq 2.58$ is clearly found.

5. Acknowledgements

This work was supported in part by the National Science Council of the Republic of China (Taiwan) under Contract No. NSC 101-2221-E-260-038-.

REFERENCES

- [1] H. M. Spivac, "Vortex Frequency and Flow Pattern in the Wake of Two Parallel Cylinders at Varied Spacing Normal to An Airstream," *Journal of the Aeronautical Sciences*, Vol. 13, 1946, pp. 289-301.
- [2] P. W. Bearman and A. J. Wadcock, "The Interference between A Pair of Circular Cylinders Normal to A Stream," *Journal of Fluid Mechanics*, Vol. 61. No. 3, 1973, pp. 499-511. [doi:10.1017/S0022112073000832](https://doi.org/10.1017/S0022112073000832)
- [3] M. M. Zdravkovich, "Review of Flow Interference Between Two Circular Cylinders in Various Arrangements," *ASME*, Vol. 99, No. 4, 1977, pp. 618-633. [doi:10.1115/1.3448871](https://doi.org/10.1115/1.3448871)
- [4] C. H. K. Williamson, "Evolution of a Single Wake behind A Pair of Bluff Bodies," *Journal of Fluid Mechanics*, Vol. 159, 1985, pp. 1-18. [doi:10.1017/S002211208500307X](https://doi.org/10.1017/S002211208500307X)
- [5] H. J. Kim and P. A. Durbin, "Investigation of the Flow between a Pair of Circular Cylinders in the Flopping Regime," *Journal of Fluid Mechanics*, Vol. 196, 1988, pp. 431-448. [doi:10.1017/S0022112088002769](https://doi.org/10.1017/S0022112088002769)
- [6] D. Sumner, S. S. T. Wong, S. J. Price and M. P. Paidoussis, "Fluid Behavior of Side-by-side Circular Cylinders in Steady Cross-flow," *Journal of Fluids and Structures*, Vol. 13. No. 3, 1999, pp. 309-339. [doi:10.1006/jfls.1999.0205](https://doi.org/10.1006/jfls.1999.0205)

- [7] Y. Zhou, H. J. Zhang and M. W. Yiu, "The Turbulent Wake of Two Side-by-side Circular Cylinders," *Journal of Fluid Mechanics*, Vol. 458, 2002, pp. 303-332. [doi:10.1017/S0022112002007887](https://doi.org/10.1017/S0022112002007887)
- [8] S. J. Xu, Y. Zhou and R. M. C. So, "Reynolds Number Effects on the Flow Structure behind Two Side-by-side Cylinders," *Physics of Fluids*, Vol. 15. No. 5, 2003, pp. 1214-1219. [doi:10.1063/1.1561614](https://doi.org/10.1063/1.1561614)
- [9] S. Kang, "Characteristics of Flow over Two Circular Cylinders in A Side-by-side Arrangement at Low Reynolds Numbers," *Physics of Fluids*, Vol. 15, 2003.
- [10] S. Kumar, B. Gonzalez and O. Probst, "Flow Past Two Rotating Cylinders," *Physics of Fluids*, Vol. 23, No. 1, 2011, 01402. [doi:10.1063/1.3528260](https://doi.org/10.1063/1.3528260)
- [11] Md Mahbub Alam, Y. Zhou, and X. W. Wang, "The Wake of Two Side-by-side Square Cylinders," *Journal of Fluid Mechanics*, Vol. 669, 2011, pp. 432-471. [doi:10.1017/S0022112010005288](https://doi.org/10.1017/S0022112010005288)
- [12] D. Sumner, "Two Circular Cylinders in Cross-flow: A Review," *Journal of Fluids and Structures*, Vol. 26. No. 6, 2010, pp. 849-899. [doi:10.1016/j.jfluidstructs.2010.07.001](https://doi.org/10.1016/j.jfluidstructs.2010.07.001)
- [13] J. Mizushima and Y. Ino, "Stability of Flows Past A Pair of Circular Cylinders in A Side-by-side Arrangement," *Journal of Fluid Mechanics*, Vol. 595, 2008, pp. 491-507. [doi:10.1017/S0022112007009433](https://doi.org/10.1017/S0022112007009433)
- [14] Y. F. Peng, A. Sau, R. R. Hwang, W. C. Yang and C. M. Hsieh, "Criticality of Flow Transition behind Two Side-by-side Elliptic Cylinders," *Physics of Fluids*, Vol. 24. No. 3, 2012, 034102. [doi:10.1063/1.3687450](https://doi.org/10.1063/1.3687450)
- [15] Y. F. Peng, R. Mittal, A. Sau and R. Hwang, "Ested Cartesian Grid Method in Incompressible Viscous Fluid Flow," *Journal of Computational Physics*, Vol. 229, No.19, 2010, pp. 7072-7101. [doi:10.1016/j.jcp.2010.05.041](https://doi.org/10.1016/j.jcp.2010.05.041)
- [16] M. Provansal, C. Mathis and L. Boyer, "Be'nard-von Ka'rman Instability: Transient and Forced Regimes," *Journal of Fluid Mechanics*, Vol. 182, 1987, pp. 1-22. [doi:10.1017/S0022112087002222](https://doi.org/10.1017/S0022112087002222)
- [17] C. H. K. Williamson, "Oblique and Parallel Modes of Vortex Shedding in the Wake of a Circular Cylinder at Low Reynolds Numbers," *Journal of Fluid Mechanics*, Vol. 206, 1989, pp. 579-627. [doi:10.1017/S0022112089002429](https://doi.org/10.1017/S0022112089002429)
- [18] C. Norberg, "An Experimental Investigation of the Flow around a Circular Cylinder: Influence of Aspect Ratio," *Journal of Fluid Mechanics*, Vol. 258, 1994, pp. 287-316. [doi:10.1017/S0022112094003332](https://doi.org/10.1017/S0022112094003332)
- [19] C. P. Jackson, "A Finite-element Study of the Onset of Vortex Shedding in Flow past Variously Shaped Bodies," *Journal of Fluid Mechanics*, Vol. 182, 1987, pp. 23-45. [doi:10.1017/S0022112087002234](https://doi.org/10.1017/S0022112087002234)
- [20] B. Kumar and S. Mittal, "Effect of Blockage on Critical Parameters for Flow past A Circular Cylinder," *International Journal for Numerical Methods in Fluids*, Vol. 50. No. 8, 2006, pp. 987-1001. [doi:10.1002/flid.1098](https://doi.org/10.1002/flid.1098)
- [21] J. Dusek, P. Le Gal and P. Fraunie, "A Numerical and Theoretical Study of the First Hopf Bifurcation in A Cylinder Wake," *Journal of Fluid Mechanics*, Vol. 264, 1994, pp. 59-80. [doi:10.1017/S0022112094000583](https://doi.org/10.1017/S0022112094000583)